Supplementary Information

Uranium-bridged Dimeric Keggin-type Polyoxometalate and its Proton Conductive Properties

Yuting Wei, Weixin Du, Haiying Wang*, Xiaoyue Wang, Keqin Shen, Minghui Xiong, Dongdi Zhang*

Henan Key Laboratory of Polyoxometalate Chemistry, College of Chemistry and Molecular Sciences, Henan University, Kaifeng, Henan 475004, China.

Experimental

General methods and materials

All reagents and solvents were of commercially available grade and used without any previous purification. *Caution! Although isotopically depleted uranium was used for all experiments described here, appropriate precautions are essential for handling all radioactive materials.* The precursor $(NH_4)_{18}[NaSb_9W_{21}O_{63}]\cdot 24H_2O$ ($\{Sb_9W_{21}\}$) was prepared according to the literature.[1] Powder X-ray diffraction (PXRD) patterns were collected on a Bruker D8 Advance instrument with Cu K_α radiation (λ = 1.5418 Å) in the angular range 2ϑ = 5-50° at 298 K. Thermogravimetric analyses (TGA) were carried out on a SDT 650 thermal analyzer under N_2 atmosphere with 10 °C min^{-1} heating rate. Infrared ray (IR) spectra were recorded on a TENSOR II spectrometer in the 4000-400 cm^{-1} range using crystalline sample in KBr pellets. Raman spectra were performed on an RM5 spectrometer (Edinburgh Instrument) from 1200 to 400 cm^{-1}. Solid-state ultraviolet-visible spectrophotometer (UV-vis) were proceeded on a Cary 5000 UV-vis in the range of 200-800 nm. Proton conductivity measurements were tested using Solartron 1260 and 1296 impedance phase gain analyzers, and the scanning frequencies ranged from 10 MHz to 0.01 Hz with a voltage of 0.1 V. Elemental analyses were performed on a Vario EL cube Elemental Analyzer and ICP-OES Agilent 5110.

X-ray crystallography

Single-crystal X-ray diffraction data was collected on a Bruker Apex-II CCD diffractometer equipped with monochromatized Mo-Kα radiation (λ = 0.71073 Å) at 150 K. The structure was solved by direct methods, and non-H atoms were refined anisotropically by full-matrix least-squares techniques against F_o^2 using the SHELXL program through the *OLEX$_2$* interface.[2] The structure was examined using the Addsym subroutine of PLATON to ensure that no additional symmetry could be applied to the models. Some disorder solvent molecules were removed through *SQUEEZE*.[3] Crystal data as well as details of the data collection and refinement for **{U_2Sb_4}** is summarized in Table S1. CCDC contains the supplementary crystallographic data for **{U_2Sb_4}** with deposition number 2369421. The crystallographic data can be obtained free of charge from The Cambridge Crystallographic Data Center via http://www.ccdc.cam.ac.

uk/data_request/cif.

Synthesis of {U_2Sb_4}

$(NH_4)_{10}[(SbW_9O_{33})_2(UO_2)_2(H_2O)_2(SbOH)_2]\cdot 7H_2O$: {$Sb_9W_{21}$} (0.24 g, 0.04 mmol) and $Na_2WO_4\cdot 2H_2O$ (0.05 g, 0.15 mmol) were dissolved in 20.0 mL of water. The pH of the resulting solution was adjusted to 4.8 using 6 mol L^{-1} HAC. Subsequently, $UO_2(NO_3)_2\cdot 6H_2O$ (0.10 g, 0.20 mmol) was added to the solution. The resulting solution turned yellow immediately. The pH of the solution was adjusted to 3.1 via 3 mol L^{-1} HCl. And then 1.64 g NH_4Cl was added. Finally, the resulting solution was stirred at 50 °C for 1.0 h. After cooled to room temperature, the solution was filtered into a beaker. Evaporation of the filtrate under ambient conditions afforded the yellow block-shaped crystals of **{U_2Sb_4}** with ca. two weeks (Yield: 8 %, based on $UO_2(NO_3)_2\cdot 6H_2O$). Elemental analysis %: calcd.: N, 2.43, Sb, 8.44, W, 57.36; found: N, 2.35, Sb, 8.52, W, 59.20. The number of guest crystal waters are calculated on the basis of TGA results.

Table S1 Crystal data and structure refinement of **{U_2Sb_4}**.

Formula	$N_{10}H_{60}O_{81}Sb_4U_2W_{18}$
Formula weight	5768.71
Temperature / K	150
Crystal system	triclinic
Space group	*P*-1
a / Å	11.5231(4)
b / Å	19.0495(6)
c / Å	21.0886(7)
α / °	89.1980(10)
β / °	89.5610(10)
γ / °	83.9440(10)
Volume / Å^3	4602.8(3)
Z	2
D_c / g cm^{-3}	3.967
μ / mm^{-1}	27.130
F(000)	4674.0
Crystal size / mm^3	0.15 × 0.1 × 0.08
2ϑ range for data collection / °	3.956 to 56.738
Limiting indices	−15 ≤ h ≤ 15, −25 ≤ k ≤ 25, −28 ≤ l ≤ 28
Reflections collected	118875

Independent reflections	R_{int} = 0.0634, R_{sigma} = 0.0487
Data/restraints/parameters	22956/1064/906
Goodness-of-fit on F^2	1.049
Final R indexes [$I >= 2\sigma (I)$]	$^aR_1$ = 0.0342, $^bwR_2$ = 0.0872
Final R indexes [all data]	$^aR_1$ = 0.0392, $^bwR_2$ = 0.0900

$^aR_1 = \sum||F_o| - |F_c||/\sum|F_o|$. $^bwR_2 = \{\sum[w(F_o^2 - F_c^2)^2]/\sum[w(F_o^2)^2]\}^{1/2}$

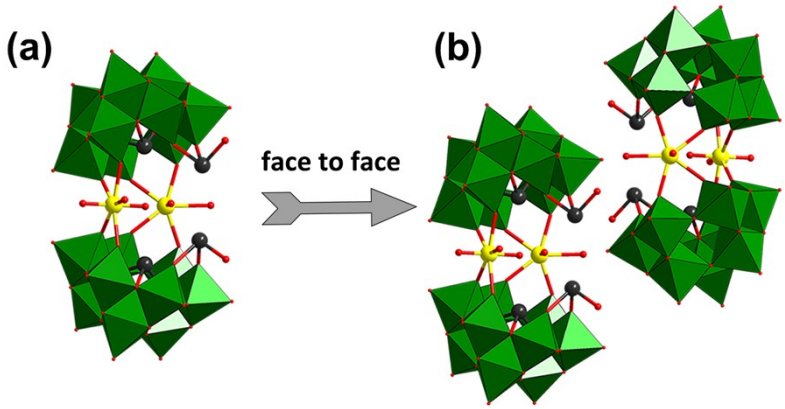

Fig. S1 The adjacent {$\mathbf{U_2Sb_4}$} polyanions are arranged "face to face". Code: {WO_6}, green octahedra; U, yellow spheres; W, green spheres; O, red spheres; Sb, dark grey spheres.

Table S2 U-O Bond lengths in **{U_2Sb_4}**.

U-O	Length/Å	U-O	Length/Å
U1–O29	1.782(6)	U2–O73	1.770(0)
U1–O92	1.783(6)	U2–O12	1.774(5)
U1–O82	2.324(6)	U2–O52	2.336(6)
U1–O10	2.331(5)	U2–O54	2.338(6)
U1–O59	2.330(6)	U2–O36	2.375(6)
U1–O49	2.345(6)	U2–O80	2.393(66)
U1–O63	2.483(6)	U2–O27	2.522(6)

Table S3 Comparison of bond lengths between **{U_2Sb_4}** and **{U_2Sb_2}**.

U_2Sb_4				**U_2Sb_2**			
M-O	Length/Å	M-O	Length/Å	M-O	Length/Å	M-O	Length/Å
U1–O29	1.782(6)	U2–O73	1.770(0)	U1–O70	1.767(2)	U2–O74	1.770(3)
U1–O92	1.783(6)	U2–O12	1.774(5)	U1–O71	1.783(1)	U2–O73	1.770(5)
U1–O82	2.324(6)	U2–O52	2.336(6)	U1–O2	2.311(3)	U2–O3	2.301(5)

U1–O10	2.331(5)	U2–O54	2.338(6)	U1–O1	2.338(4)	U2–O8	2.339(6)
U1–O59	2.330(6)	U2–O36	2.375(6)	U1–O5	2.353(5)	U2–O4	2.356(8)
U1–O49	2.345(6)	U2–O80	2.393(66)	U1–O6	2.375(8)	U2–O7	2.378(4)
U1–O63	2.483(6)	U2–O27	2.522(6)	U1–O72	2.508(1)	U2–O75	2.485(6)
Sb1–O58	1.993(6)	Sb3–O60	1.972(6)	Sb1–O17	1.980(0)	Sb2–O41	1.978(3)
Sb1–O90	1.997(6)	Sb3–O72	2.002(6)	Sb1–O12	1.991(2)	Sb2–O46	1.991(2)
Sb1–O62	1.999(5)	Sb3–O46	2.057(6)	Sb1–O20	2.009(6)	Sb2–O49	1.999(3)
Sb2–O32	1.957(6)	Sb4–O94	1.987(6)				
Sb2–O68	2.000(6)	Sb4–O14	1.992(5)				
Sb2–O8	2.066(6)	Sb4–O64	1.999(6)				

Table S4 Bond valence sum calculations for U, Sb, W and O atoms in **{U_2Sb_4}**.

Atom	BVS	Atom	BVS	Atom	BVS	Atom	BVS
U1	6.30	O4	1.76	O38	1.87	O67	1.71
U2	6.28	O12	2.12	O40	1.94	O68	0.93[#]
Sb1	2.83	O13	1.72	O41	1.68	O69	1.72
Sb2	2.74	O14	2.05	O42	1.94	O70	1.89
Sb3	2.72	O15	1.67	O44	2.08	O71	1.66
Sb4	2.86	O16	1.99	O46	1.96	O72	2.06
W1	6.16	O17	1.66	O48	1.89	O73	2.14
W2	6.15	O18	1.88	O49	1.87	O76	1.98
W3	6.07	O19	1.72	O50	2.02	O77	1.75
W4	6.20	O20	1.81	O51	1.64	O78	1.80
W5	6.08	O22	1.84	O52	1.86	O80	1.84
W6	6.11	O24	1.85	O54	1.90	O82	1.85
W7	6.13	O25	2.01	O55	1.93	O84	1.77
W8	6.15	O26	1.86	O56	2.05	O86	2.05
W9	6.06	O27	0.28*	O57	1.69	O88	2.02
W10	6.08	O28	1.79	O58	2.10	O90	2.07
W11	6.21	O29	2.07	O59	1.94	O92	2.06
W12	6.09	O30	1.77	O60	1.00[#]	O94	2.11
W13	6.06	O31	1.74	O61	1.65	O96	1.83
W14	6.10	O32	2.09	O62	2.03	O97	1.86
W15	6.17	O33	1.69	O63	0.31*	O98	2.07
W16	6.11	O34	2.00	O64	1.99		
W17	6.10	O36	1.84	O65	1.68		
W18	6.15	O37	1.74	O66	1.75		

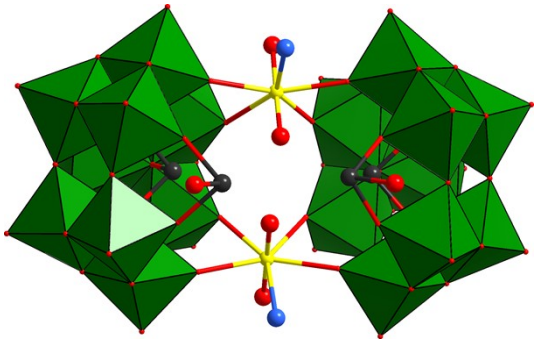

Fig. S2 Polyhedral and ball-and-stick representation of **{U_2Sb_4},** the coordinated water molecules (O_{27} and O_{63}) are highlighted in blue. Code: {WO_6}, green octahedra; U, yellow spheres; W, green spheres; O, red spheres; Sb, dark grey spheres.

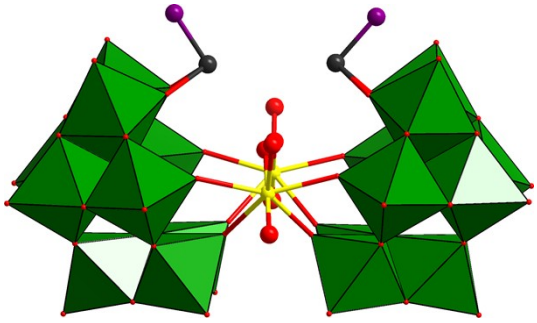

Fig. S3 Polyhedral and ball-and-stick representation of **{U_2Sb_4}**, the monoprotonated O_{60} and O_{68} are highlighted in violet. Code: {WO_6}, green octahedra; U, yellow spheres; W, green spheres; O, red spheres; Sb, dark grey spheres.

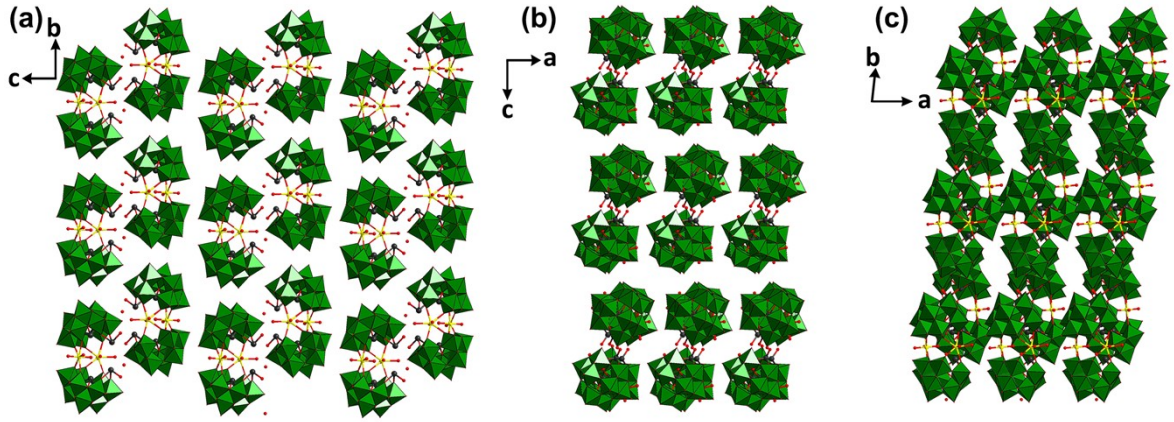

Fig. S4 The packing diagram of **{U_2Sb_4}** in different directions. Code: {WO_6}, green octahedra; U, yellow spheres; W, green spheres; O, red spheres; Sb, dark grey spheres.

Table S5 The proton conductivities recently reported polyoxometalates.

Formula	σ / S·cm^{-1}	conditions	Refs
$H_{17}\{(H_2en)_3[Sb^{III}_9Sb^{V}Ce_3O_{14}(H_2O)_3][(SbW_9O_{33})_3(PW_9O_{34})]\}\cdot 28H_2O$	4.57×10^{-4}	85 °C, 98 % RH	4
$H_{13}\{(HIm)_4K_2Na_4[Sb^{III}_9Sb^{V}Sm_3O_{14}(H_2O)_3][(SbW_9O_{33})_3(PW_9O_{34})]\}\cdot 26H_2O$	1.64×10^{-2}	85 °C, 98 % RH	4
$K_8Na_3Li_5\{[Na(NO_3)(H_2O)]_4[Al_{16}(OH)_{24}(H_2O)_8(P_8W_{48}O_{184})]\}\cdot 66H_2O$	4.50×10^{-2}	85 °C, 70 % RH	5
$K_{11}Li_9(NH_4)_4[Ga_{16}(OH)_{32}(P_8W_{48}O_{184})]\cdot 112H_2O$	7.90×10^{-3}	85 °C, 70 % RH	5
$Na_{17}K_{14}(H_2pip)_{10}H_8\{La_{27}Ge_{10}W_{106}O_{406}(OH)_4(H_2O)_{24}\}\cdot nH_2O$ (n≈130)	1.5×10^{-2}	85 °C, 98 % RH	6
$Na_8K_4(H_2pip)_8H_{21}\{[Cu(pip)_2]_2[La_{29}Ge_{10}W_{106}O_{406}(OH)_4(H_2O)_{28}]\}\cdot nH_2O$ (n≈127)	5.3×10^{-3}	85 °C, 98 % RH	6
$H_5K_3Na[Cu(en)_2]_2[Cu(en)_{0.75}(H_2O)_{2.5}]\{[(Te_2Nb_{19}O_{58})(\mu_3\text{-}OH)_2]\}\cdot 24H_2O$	7.90×10^{-3}	85 °C, 98 % RH	7

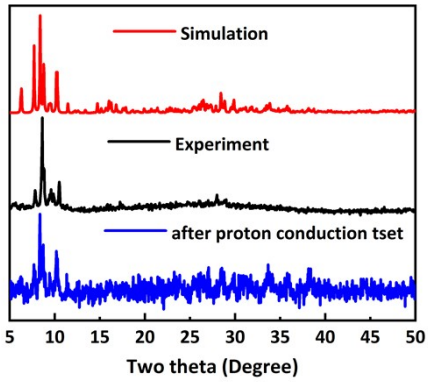

Fig. S5 PXRD patterns of **{U_2Sb_4}** with simulated (black), experimental (red) and after proton conduction (blue). The main peaks are retained after the proton conduction tests with slight changes in the morphology.

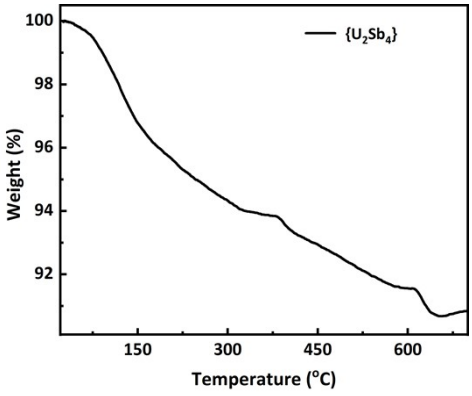

Fig. S6 The TG curve of **{U_2Sb_4}**.

The TG curve of **{U_2Sb_4}** shows two steps for the weight loss process. The first step from 25 °C to 350 °C corresponds to the loss of crystal lattice water, coordinated water molecules and 10 ammonium ions. TG analysis is performed to examine the thermal stability and determine the number of lattice water molecules in **{U_2Sb_4}**. After 350 °C, the metal skeleton gradually decomposes, leaving metal oxides.

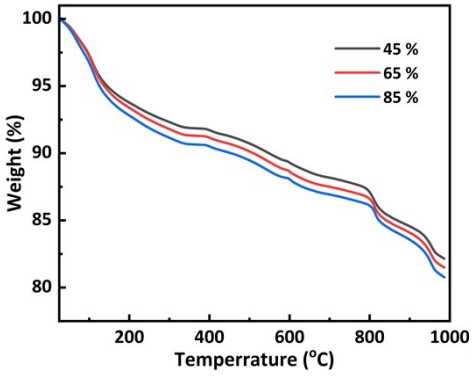

Fig. S7 TG curves after exposing to different humidity environments.

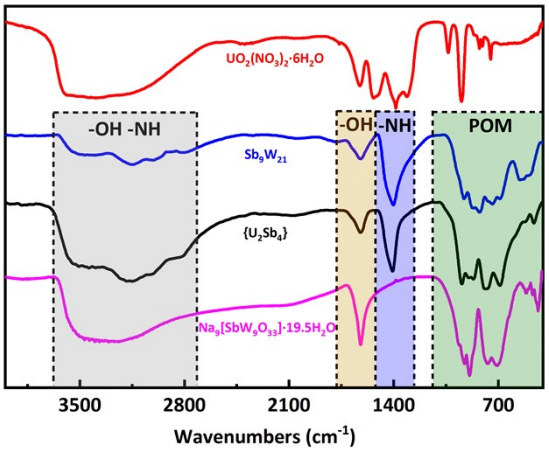

Fig. S8 The IR spectra of $UO_2(NO_3)_2·6H_2O$, $\{Sb_9W_{21}\}$, **$\{U_2Sb_4\}$** and $Na_9[SbW_9O_{33}]·19.5H_2O$.

As shown in Fig. S8, **$\{U_2Sb_4\}$** has strong absorption peaks in the range of 500-1000 cm^{-1}, corresponding to the characteristic peaks of the trilacunary Keggin-type $[SbW_9O_{33}]^{9-}$ skeleton. The absorption peaks at 943, 898, 864, 801 and 772 cm^{-1} correspond to the characteristic peaks of $\nu(W\text{-}O_d)$, $\nu(W\text{-}O_b\text{-}W)$ and $\nu(W\text{-}O_c\text{-}W)$, respectively.[8] The stretching vibration peak of the uranyl bond is about 850 cm^{-1}, which overlaps with the stretching vibration peak of $\nu(W\text{-}O)$ and is therefore not observed.[9] The vibration at 1406 and 1618 cm^{-1} related to NH_4^+ and the bending vibration of -OH.[10] The characteristic bands from 3600 to 2700 cm^{-1}, corresponding to the overlapped stretching of -OH and -NH, respectively.

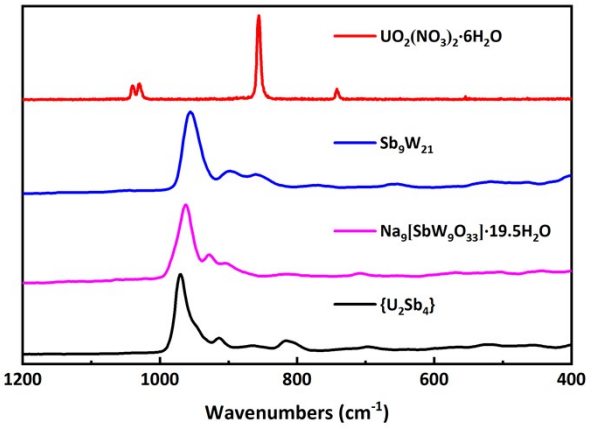

Fig. S9 The Raman spectra of $UO_2(NO_3)_2{\cdot}6H_2O$, $\{Sb_9W_{21}\}$, $Na_9[SbW_9O_{33}]{\cdot}19.5H_2O$ and **$\{U_2Sb_4\}$**.

The Raman spectra show signals for *ν*(W-O) at 957, 906, 967, 913 and 815 cm^{-1} [11]. The signal at 815 cm^{-1} is the symmetric stretching vibration peak of O=U=O. Compared with the stretching vibration peak at 860 cm^{-1} in $UO_2(NO_3)_2{\cdot}6H_2O$[12], the position of the characteristic peak of uranyl bond in **$\{U_2Sb_4\}$** shows an obvious blue shift. This is mainly due to the coordination of uranium with trilacunary Keggin-type $[SbW_9O_{33}]^{9-}$ unit through the oxygen atom on the equatorial plane, which increases the electron density of the U(VI) center.[13]

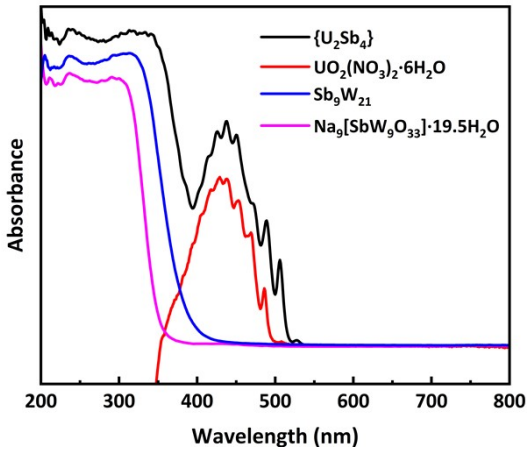

Fig. S10 The Solid-UV-vis spectra of **$\{U_2Sb_4\}$**, $UO_2(NO_3)_2{\cdot}6H_2O$, $\{Sb_9W_{21}\}$ and $Na_9[SbW_9O_{33}]{\cdot}19.5H_2O$.

As shown in the Solid-UV-vis spectra, an absorption peak was observed for UO_2^{2+} in 350-550 nm, which belongs to $O_{2p}\rightarrow U_{5f}$ charge transfer.[14] The absorption peak between 200-350 nm belongs to the pπ–dπ charge transfer transition of O_t–W bonds.[15]

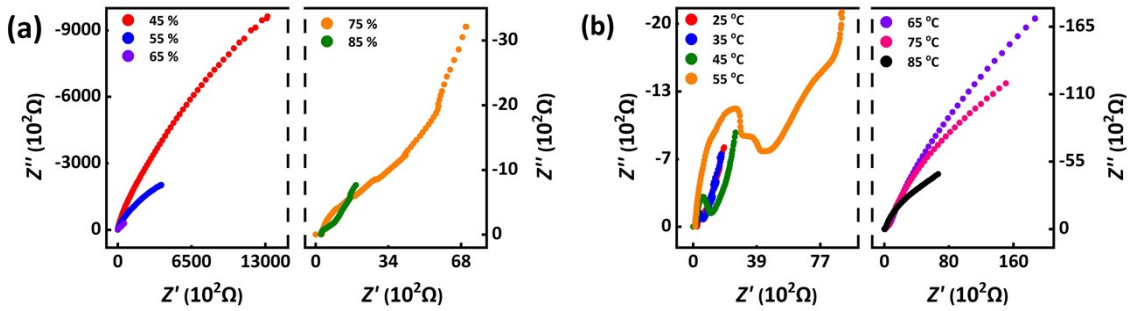

Fig. S11 The Nyquist plots of **{U_2Sb_4}** at 25 °C with 45-85 % RHs (a) and 85 % RH with 25-85 °C (b).

Proton conductivity test experimental section

The powder sample was placed into a 3 mm diameter mold and pressed into pellet with a thickness of about 0.1 mm under a pressure of 0.5 MPa, held for 2 min. Subsequently, the pellet was fixed on the sample stage with silver colloid, and gold wires were applied to both sides. Proton conductivities was determined using an impedance and gain-phase analyzer (Solartron 1260/1296) with an input voltage 100 mV in the frequency range 10 MHz to 0.01 Hz, under a constant temperature and humidity conditions. The measured temperature ranged from 25 °C to 85 °C, and the relative humidity (RH) ranged from 45 % to 85 %. In the measurement of the RH dependence of conductivity, a time interval of 14.5 h, 18.5 h, 21 h, 27 h, and 38 h is set between placing the sample in the measurement chamber and measuring the value.

Proton conductivity was calculated using the following equation:

$$\sigma = L / RS$$

Where σ is the conductivity (S cm^{-1}), L is the thickness (cm) of the pellet, S is the crosssectional area (cm^2) of the pellet and R is the bulk resistance (Ω). The resistance values can be obtained by impedance analysis Zview software.

The mechanism of proton conduction was investigated by calculating the activation energy (E_a) corresponding to proton conduction at different temperatures using the Arrhenius equation, which is as follows:

$$\sigma T = \sigma_0 \exp(-E_a / k_b T)$$

where σ_0 is the pre-exponential factor, k_b is the Boltzmann constant (eV / K) and T is the temperature (K).

References

(S1) G. Hervéa, A. Téazéa, J. Liu and M. T. Pope, *Inorganic Syntheses*, 1990, **27**, 118–120.

(S2) O. V. Dolomanov, L. J. Bourhis, R. J. Gildea, J. A. K. Howard and H. Puschmann, *J. Appl. Crystallogr*, 2009, **42**, 339–341.

(S3) A. L. Spek, *Acta Cryst. C.*, 2015, **71**, 9–18.

(S4) H.-P. Xiao, R.-T. Zhang, Z. Li, Y.-F. Xie, M. Wang, Y.-D. Ye, C. Sun, Y.-Q. Sun, X.-X. Li and S.-T. Zheng, *Inorg. Chem.,* 2021, **60**, 13718−13726.

(S5) P. Yang, M. Alsufyani, A. Emwas, C. Chen and N. M. Khashab, *Angew. Chem. Int. Ed.*, 2018, **57**, 13046–13051.

(S6) Z. Li, X. Li, T. Yang, Z. Cai and S. Zheng, *Angew. Chem. Int. Ed.*, 2017, **56**, 2664–2669.

(S7) P.-X. Wu, Y. Han, Y.-J. Lin, Y.-Q. Sun and S.-T. Zheng, *Dalton Trans.*, 2024, **53**, 7424–7429.

(S8) S. Duval, S. Sobanska, P. Roussel and T. Loiseau, *Dalton Trans.*, 2015, **44**, 19772–19776.

(S9) M. Dufaye, S. Duval, G. Stoclet, X. Trivelli, M. Huvé, A. Moissette and T. Loiseau, *Inorg. Chem.*, 2019, **58**, 1091–1099.

(S10) M. Croce, S. Conti, C. Maake and G. R. Patzke, *Eur. J. Inorg. Chem.*, 2019, **2019**, 348–356.

(S11) C. Zhao, E. N. Glass, B. Chica, D. G. Musaev, J. M. Sumliner, R. B. Dyer, T. Lian and C. L. Hill, *J. Am. Chem. Soc.*, 2014, **136**, 12085–12091.

(S12) J. M. Wabwile, H. K. Angeyo and A. D. Massop, *J. Environ. Radioact.*, 2023, **270**, 107295.

(S13) N. M. Byrne, M. H. Schofield, A. D. Nicholas and C. L. Cahill, *Dalton Trans.*, 2021, **50**, 9158–9172.

(S14) M. Mohadeszadeh, *J. Clust. Sci.*, 2011, **22**, 183–192.

(S15) Sun, Y. Zou, H. Li, W. Chen, P. Ma, J. Niu and J. Wang, *Inorg. Chem.*, 2024, **63**, 2363–2369.